AN EXPERIMENTAL INVESTIGATION OF SOLID OXIDE FUEL CELL PERFORMANCE AT VARIABLE OPERATING CONDITIONS

by

Ismet TIKIZ and Imdat TAYMAZ*

Department of Mechanical Engineering, University of Sakarya, Adapazari, Turkey

Original scientific paper
DOI: 10.2298/TSCI130617019T

Cell temperature and selection of the reactant gases are crucial parameters for the design and optimization of fuel cell performance. In this study, effect of operating conditions on the performance of solid oxide fuel cell has been investigated. Application of response surface methodology was applied to optimize operations conditions in solid oxide fuel cell. For this purpose, an experimental set-up for testing of solid oxide fuel cell has been established to investigate the effect of hydrogen, oxygen, nitrogen flow rates and cell temperature parameters on cell performance. Hydrogen flow rate, oxygen flow rate, nitrogen flow rate, and cell temperature were the main parameters considered and they were varied between 0.25 and 1 L/min, 0.5 and 1 L/min, 0 and 1 L/min, and 700-800 ºC in the analyses, respectively. The maximum power density was found as 0.572 W/cm^2 in the experiments.

Keywords: *fuel cell, solid oxide fuel cell, cell performance*

Introduction

Fuel cells are electrochemical devices that convert the chemical energy stored in a fuel directly into electrical power. The most common classification methods of fuel cells are electrolyte type, operating temperatures, and the charge mechanism. Solid oxide fuel cell (SOFC) have potential to be the cleanest and the most efficient devices for cost-effective conversion of a wide variety of fuels, including hydrogen, hydrocarbons, coal gas, and bio-derived renewable fuels to electricity. Also, SOFC are particularly attractive due to their special features such as: great fuel flexibility, the feasibility of fuel internal reforming, high energy conversion efficiency, low emission noise, and the potential applicability in the highly efficient co-generation power systems. Furthermore, with the increasingly visible multi-fuel capability, SOFC are being paid more attention recently [1-4]. The SOFC are classified according to their shapes: planar, cylindrical, and flat-tube fuel cells. Planar SOFC provide low electronic resistance and easy stacking, but it is difficult to prevent gas leakage. Modeling and optimization can play an important role towards these goals. There is a need for accurate models suitable for optimization that will allow the exploration of the design space in a fast and accurate way.

* Corresponding author; e-mail: taymaz@sakarya.edu.tr

However, further development of the planar SOFC faces challenges related to maximizing the power density and minimizing the non-uniform distribution of temperature, which contributes to thermal stress in the SOFC components. Nowadays, SOFC are still not commercially available mainly because of their high manufacturing costs and low durability [5-8].

There have been numerous studies in recent years on SOFC. Costamagna *et al*. [9] investigated basic unit of a modular plant which is containing an electro-chemical reactor formed by a number of integrated planar SOFC modules, and a reforming reactor. Razbani *et al*. [10] analyzed the effect of current and oven temperature on SOFC performance. Increasing current density results in higher temperature gradient. Higher oven temperatures, on the other hand, improve temperature uniformity. Yan *et al*. [11] built a 3-cell stack of anode supported planar SOFC to evaluate the application of an external-manifold design. Also, a two-cell planar stack at the Julich Institute of Energy and Climate Research in Germany F-design with solid oxide cells was investigated by [12]. Jin *et al*. [13] presented effect of contact area and depth between cell cathode and interconnect on output power density and degradation of stack for planar SOFC systematically. The results indicate that the maximum output power density of repeating units inside stack increases firstly and then decreases slightly with the increasing interface contact area and depth, respectively. Djamel *et al*. [14] investigated the effect of the hydrogen and the air temperature values on the temperature distribution in a planar SOFC with the aid of a 2-D mathematical model. Kim *et al*. [15] performed high-temperature electrolysis with various gas compositions to investigate the effects of the hydrogen partial pressure and the humidity generated by the steam electrode on the performance and durability of solid oxide electrolysis cells. The power density of the button cell used in this research was 0.48 W/cm^2 at 750 ºC, and the flow rates of the air and humidified hydrogen were 100 cm^3 per minute. Lima *et al*. [16] fabricated a large-area (10 cm × 10 cm) anode-supported SOFC and tested in a single cell stack. The gas over potential can be depressed by increasing the fuel flow rate, *i. e*., enhancing the effective gas exchange over the anode. It is important to distinguish this additional over potential due to operating conditions such as gas flow rate and gas composition from the other polarization phenomenon caused by the electrochemical performance of the anode itself. In the review papers, the application of SOFC technology in power generation sector studied by [17] and Secanella *et al*. [18] discussed the strengths, limitations, advantages, and disadvantages of optimization formulations and numerical, optimization algorithms, and insight obtained from previous studies. The new cathode processing technique is presented by Ortiz-Vitoriano *et al*. [19] provides a more economical, lower temperature SOFC production route with no detrimental effect on device efficiency. The CFD method was used by [20, 21] to perform for the flow distribution in planar SOFC. The calculations were based on 3-D models with realistic geometric and operational parameters. The effects of design parameters, such as the channel height and length, the height of the repeating cell unit and the manifold width, on the flow uniformity were examined.

In the previous mentioned literature, most of the SOFC studies mainly focus on the effect of the cell temperature and reactant flow rate parameters on the performance. Defining of operation condition, limited and expensive components and high experimental and commercial systems cost are mainly disadvantages of the research of fuel cells. In order to eliminate such kind of factors, predetermination of alternative parameters gets time and economic benefit. Recently, some statistical techniques like response surface methodology (RSM) has been using for analyzing the effects of several independent variables on the dependent variables. Modeling and optimization can play an important role towards these goals. There is a need for accurate models suitable for optimization that will allow the exploration of the design space in a fast and accurate way.

Few researchers, who are working about polymer electrolyte membrane type fuel cells [22] and direct methanol type fuel cells [23], applied RSM to their studies. But, this methodology has not been applied for SOFC studies. In this study, SOFC model was analyzed by using RSM to find suitable parameters and to optimize operation conditions.

Governing equations of SOFC

Fuel cells are devices that convert the chemical energy contained in a fuel electrochemically into electrical energy. The basic physical structure of a fuel cell consists of an electrolyte layer in contact with an anode and a cathode on either side [24]. In a typical fuel cell, fuel is fed continuously to the anode (negative electrode) and an oxidant (oxygen or air) is fed continuously to the cathode (positive electrode). The electrochemical reactions take place at the electrodes to produce an electric current through the electrolyte, while driving a complementary electric current that performs work on the load.

A schematic view of SOFC components is shown in fig. 1. A planar SOFC consists of anode gas channel, anode gas diffusion electrode (GDE), anode interlayer (active electrode), electrolyte, cathode interlayer (active electrode), cathode GDE, and cathode gas channel. Using component materials in the study are 10 mol scandium oxide doped zirconium oxide (ScSZ) for electrolyte, NiO-ScSZ composite materials for anode electrode and LSM-ScSZ composite materials for cathode electrode.

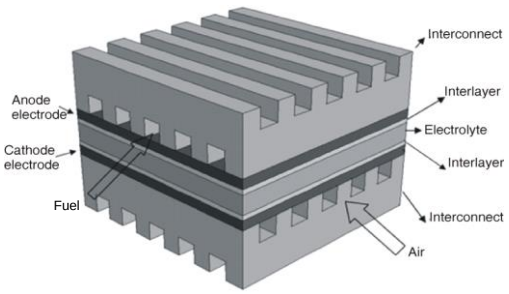

Figure 1. A schematic view of SOFC components

The electro-chemical reactions are considered to occur at the active regions of the porous electrodes (*i. e*. interlayer). In a SOFC, oxidant reduction occurs in the active cathode. The oxygen ion is then transported through the electrolyte and then in the active anode oxidation of the fuel occurs by following reactions [25].

Using general governing equations during fuel cell operation are:

$$\text{Anode:} \quad H_2 + O^{-2} \rightarrow H_2O + 2e^-$$

$$\text{Cathode:} \quad \tfrac{1}{2}O_2 + 2e^- \rightarrow O^{-2}$$

$$\text{Overall:} \quad H_2 + \tfrac{1}{2}O_2 \rightarrow H_2O$$

Mass conservation

The mass conservation equation (or continuity equation) simply requires that the rate of mass change in a unit volume must be equal to the sum of all the species entering (exiting) the volume in a given time period.

$$\frac{\partial}{\partial t}(\varepsilon\rho) + \nabla(\varepsilon\rho U) = 0$$

The previous equation is modified and expressed:

$$\nabla(\rho U) = S_{\text{mass}}$$

where ρ [kgm^{-3}] is the density, U [ms^{-1}] – the velocity, ε – the porosity implemented in this equation to account for porous domains such as electrode and gas channels, and S_{mass} – the source term. In the mass conservation equation it has different source terms in different cell zones. At the electrode/electrolyte interface, there are hydrogen/oxygen consumption and water formation. The mass sink and source rate depend on the electrochemical reaction rates. Thus they can be calculated by:

$$S_{\text{H}_2} = -\frac{M_{\text{w,H}_2}}{2F} i_{\text{an}}$$

$$S_{\text{O}_2} = -\frac{M_{w,\text{O}_2}}{4F} i_{cat}$$

$$S_{\text{H}_2\text{O}} = -\frac{M_{w,\text{O}_2}}{2F} i_{cat}$$

where M_{w} is the molecular weight, i – the current density, and F – the Faraday constant (96500 C/mol).

Momentum conservation

Similarly to the mass conservation equation, we can set up an equation using vector form for momentum conservation:

$$\frac{\partial}{\partial t}(\varepsilon\rho U) + \nabla(\varepsilon\rho UU) = -\varepsilon\nabla p + \nabla(\varepsilon^{\zeta}) + \frac{\varepsilon^2\mu U}{\kappa}$$

where ζ and μ stand for the shear stress tensor and the fluid dynamic viscosity, respectively. The weakly compressible Navier-Stokes equations govern the flow in the open channels:

$$\rho(u\nabla)u = \nabla\left\{-p[\text{I}] + \frac{\mu}{\varepsilon}\left[\nabla u + (\nabla u)^T\right] - \frac{2}{3}(\nabla u)[\text{I}]\right\}$$

$$\nabla(\rho u) = Q$$

In the porous GDE, the Brinkman equation describes the flow velocity:

$$\left(\frac{\mu}{\kappa} + Q\right)u = \nabla\left\{-p[\text{I}] + \frac{\mu}{\varepsilon}\left[\nabla u + (\nabla u)^T\right] - \frac{2}{3}(\nabla u)[\text{I}]\right\}$$

$$\nabla(\rho u) = Q$$

where ε and κ [m^2] denotes the porosity and permeability of medium, respectively, [I] – the identity matrix, and Q – the mass source term, which relates to the charge transfer current density i_{ct} according to:

$$Q = \sum_i S_a \frac{i_{\text{ct},i} M_i}{n_i F}$$

where S_{a} is the specific surface area and n stands for the number of moles of electrons transferred. Solving the momentum conservation equation permits us to obtain the pressure, p, distribution of the fluids flowing through the fuel cell.

Species conservation

The mass conservation and the momentum conservation equations previous discussed are used to describe the overall bulk motion of the fluid mixture. In contrast, the species conservation equation describes the differential movement of each individual species within the fluid mixture:

$$\frac{\partial}{\partial t}\left(\varepsilon\rho x_i\right)+\nabla\left(\varepsilon\rho U x_i\right)=\nabla\left(\rho D_i^{\text{eff}}\nabla x_i\right)+\dot{S}_i$$

where x_i and D_i^{eff} [ms^{-1}] stand for species mass fraction and effective diffusivity of each species *i*. The material transport is described by the Maxwell-Stefan's diffusion and convection equation. Let ω_i be the weight fraction of species *i*. In the stationary case, the mass balance is governed by:

$$\nabla\left\{\omega_i\rho u-\rho\omega_i\sum_{j=1}^{k}\overline{\overline{D_{ij}}}\left[\frac{M}{M_j}\left(\nabla\omega_j+\omega_j\frac{\nabla M}{M}\right)+\left(x_j-\omega_j\right)\frac{\nabla p}{p}\right]\right\}=R_i$$

where $\overline{\overline{D_{ij}}}$ represents the *ij* components of the multi-component Fick diffusivity, which is calculated from the Maxwell-Stefan diffusivity, D_{ij} [ms^{-1}]:

- Fick diffusivity: $J_i=-c_t\overline{\overline{D_{ij}}}\nabla x_j$, and
- Maxwell-Stefan diffusivity: $\nabla x_i=x_i x_j\left(u_i-u_j\right)/D_{ij}$

where J_i [molm^{-2}s^{-1}] is the diffusion flux, c_t [molm^{-3}] – the total mixture molar concentration, u [ms^{-1}] – the velocity, ρ [kgm^{-3}] – the density of the fluid, p [Pa] – the pressure, and R_i [kgm^{-3}s^{-1}] – the reaction source term for species *i*, and x_j the molar fraction of species *j*. The average molecular weight is calculated:

$$M=\sum_{j=1}^{k}x_j M_j$$

where M_j [kgmol^{-1}] is the molar mass of species *j*. Assume the gas to be ideal, so that the density is given by:

$$\rho=\frac{pM}{RT}$$

In the open channel, the reaction source term is set to zero. However, in the GDE, the source term is given by the electrochemical reaction rate. It is calculated from the charge transfer current density according to the Faraday's law:

$$R_i=\nu_i\frac{i_{\text{ct},i}M_i}{n_i F}$$

where ν_i is the stoichiometric coefficient and n_i is the number of electrons in the reaction.

Energy conservation

The energy conservation equation describes the thermal balance within the fuel cell:

$$\frac{\partial}{\partial t}\left(\varepsilon\rho h\right)+\nabla\left(\varepsilon\rho U h\right)=\nabla k^{\text{eff}}\nabla T+\varepsilon\frac{\mathrm{d}p}{\mathrm{d}t}-j\eta+\frac{\hat{\hat{i}}\hat{\hat{i}}}{\sigma}+S_t$$

where h and k^{eff} stand for enthalpy of fluid flowing through the fuel cell and its effective thermal conductivity, respectively. The fluid enthalpy may be calculated based on the species present in the fluid and the fluid temperature, *T*. The first term on the retirement health savings (RHS) accounts for the rate of energy change due to thermal conditions. The second term

on the RHS accounts for rate of energy change due to the mechanical work of the fluids. In the last terms on the RHS, η, $\hat{\imath}$, σ, and S_t stand for overvoltage, current flux vector, electric conductivity and heat sources, respectively.

During the electrochemical reaction, the heat source includes the ohmic heat and reaction heat. In different zones, the heat source is different, such as in GDE, the reaction heat is the primary part; while in electrolyte, ohmic heat is the main heat source. From our basic assumptions the previous general equation is simplified:

$$\nabla\left(\rho_i U_i T\right) = \nabla\left(k^{\text{eff}} \nabla T\right) + S_t$$

where in the source term:

$$S_t = I^2 R_{\text{ohm}} + h + \eta_{\text{an}} i_{\text{an}} + \eta_{\text{cat}} i_{\text{cat}}$$

k^{eff} [$\text{Wm}^{-1}\text{K}^{-1}$] is the effective thermal conductivity, I [A] – the electric current, and R [Ω] – the electric resistance.

Experimental

Response surface methodology applied to a single SOFC

The RSM is applied different science field such as chemists, electrochemists, and materials. The experiment is designed to allow the estimation of factor interactions. Therefore, it gives an idea about the (local) shape of the investigated response surface. The SOFC designs are used to find improved or optimal process settings, troubleshoot process problems and weak points, and to make a product or a process more robust against external and non-controllable influences [26]. The RSM consists of a group of mathematical and statistical techniques that can be used to define the relationships between the response and the independent variables and helps researchers to build models, evaluate the effects of several factors and establish the optimum conditions for the desired responses [27]. It is possible to separate an optimization study using RSM into three stages. The first stage is the preliminary work in which the determination of the independent parameters and their levels are carried out. The second stage is the selection of the experimental design and the prediction and verification of the model equation. The last one is obtaining the response surface plot and contour plot of the response as a function of the independent parameters and determination of optimum points [28].

In this study, the RSM is applied to a SOFC operating at the steady-state for obtaining the power response surface. The design is generated considering four operating parameters (cell temperature, hydrogen flow rate, oxygen flow rate, and nitrogen flow rate) with different cases. In addition to analyzing the effects of these variables, by using experimental methodology [29] following mathematical (quadratic) model also is given:

$$Y = \beta_0 + \sum_{\text{I}=1}^{4} \beta_i X_i + \sum_{\text{I}=1}^{4} \beta_{ii} X_i^2 + \sum_{i=1}^{4} \sum_{j=1+i}^{4} \beta_{ij} X_i X_j + e$$

where Y is the response variable (power density), X_i – the main factors (cell temperature $i = 1$, hydrogen flow rate $i = 2$, oxygen flow rate $i = 3$, and nitrogen flow rate $i = 4$), β_i – the linear coefficients, β_0 – the constant coefficient, β_{ii} – the quadratic coefficients for the variable I, and β_{ij} – the linear model coefficients for the interaction between the variables i and j. The sets of β are unknown parameters. To estimate the values of these parameters, we must collect data on

the system we are studying. Because, in general, polynomial models are linear functions of the unknown parameters of β, we refer to the technique as linear regression analysis.

Experimental system

This experimental study has been carried out at Nigde University Department of Mechanical Engineering. It is shown that geometrical properties of single SOFC fuel cell which was used at the experiment in tab. 1. The experimental system which is shown in fig. 2 provides the control of hydrogen, oxygen and nitrogen flow rates and cell temperature for the cathode and anode.

Specification and accuracy properties of experimental apparatus are given in tab. 2.

By taking into consideration RSM results, operation parameters values are defined: cell temperature in the range of 700-800 ºC, hydrogen flow rate in the range of 0.25-1 L per minute, oxygen flow rate in the range of 0.5-1 L per minute, and nitrogen flow rate in the range of 0-0.25 L per minute.

Table 1. Geometrical properties of the experimental SOFC

Parameters	Value	Unit
Channel depth	1	mm
Channel width	40	mm
Channel length	40	mm
Active area	1600	mm^2

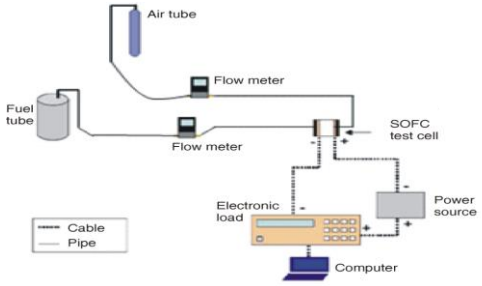

Figure 2. Schematic of experimental system

Table 2. Technical properties of experimental apparatus

Apparatus	Specification	Accuracy
Air tube	Turkish Standart Institute, No: 11169, 10 L	–
Flow meter	Alicat Scientific Incorporated, Tucson, USA	0.1 mL/min
Fuel tube	Turkish Standart Institute, No: 11169, 10 L	–
Electronic load	RIGOL DS1302CA	Single-shot: ±(1 sample interval + 50 ppm × reading + 0.6 ns)
DC power supply	GW-INSTEK GPS-2303	±(0.5% of rdg + 2 digits)
Test station	Arbin Instruments, FCTS, Texas, USA	Current and voltage accu.0.02% or 0.05% of full scale range
Thermocouple	K type Omega	Greater of 2.2 C or 0.75%

Design of experiments

The central composite design (CCD) in RSM was performed to investigate the effect of four parameters on the fuel cell performance. Cell temperature, hydrogen flow rate, oxygen flow rate, and nitrogen flow rate were selected as independent variables and power density of SOFC was selected as response variable. The CCD was implemented using Design-Expert 7.0 [30]. Experimental values of the response variables for CCD are given in tab. 3. Optimization toolbar in the Design Expert 7.0 software was used to determine the maximum power density. The uncertainties for the experimental results are calculated according to the procedure outlined by Kline and McClintock [31]. The results of the uncertainty analysis are tabulated in tab. 4.

Table 3. Experimental values of the response variables for central composite design

Run	Cell temperature [ºC]	Hydrogen flow rate [Lmin^{-1}]	Oxygen flow rate [Lmin^{-1}]	Nitrogen flow rate [Lmin^{-1}]	Power density [mWcm^{-2}]
1	750	0.625	1	0.125	410
2	800	1	1	0	572
3	750	0.625	0.75	0.125	401
4	750	0.625	0.75	0.125	399
5	700	1	1	0.25	418
6	750	1	0.75	0.125	425
7	800	0.625	0.75	0.125	212
8	700	0.25	1	0	279
9	800	0.25	0.5	0.25	40
10	750	0.625	0.75	0.25	420
11	700	1	0.5	0.25	266
12	750	0.625	0.75	0.125	380
13	750	0.25	0.75	0.125	345
14	800	0.25	1	0.25	43
15	700	0.625	0.75	0.125	255
16	800	1	0.5	0	505
17	750	0.625	0.75	0	448
18	750	0.625	0.75	0.125	392
19	750	0.625	0.75	0.125	390
20	700	0.25	0.5	0	253
21	750	0.625	0.5	0.125	378

Table 4. Summary of estimated uncertainties

Parameter	Units	Uncertainty
Temperature	°C	±0.05 °C
Flow rate	L/min.	±0.1%
Electrical Potential	mV	±0.05 mV

Results and discussion

It was used the Design Expert 7.0 software to determine the maximum power density under ambient conditions. While the criteria for the operating environment was determining, the power density was selected as the maximum degree of importance due to the goal is to achieve the maximum power density. In tab. 5, it is given that parameters selected as independent cell temperature, hydrogen flow rate, oxygen flow rate, and nitrogen flow rate is kept within the range of the study. Based on these data, the program provides a maximum power densities values are given in tab. 6. Program recommends that the number 1 test conditions out of the 21 different optimal points.

An analysis of variance (ANOVA) was performed to verify the significance of this quadratic model.

The significance of the quadratic model equation is expressed by the coefficient of determination R^2 and F value. The F value is the ratio of the model mean square/residual mean square and shows the relative contribution of the model variance to the residual variance. The model F-value of 152.47 implies the model is significant. The P-values less than 0.0001 indicate

Table 5. Operating ranges corresponding to the maximum power density

Name	Unit	Goal	Lower limit	Upper limit	Lower weight	Upper weight	Importance
Cell temperature	°C	is in range	700	800	1	1	3
Hydrogen flow rate	L/min.	is in range	0.25	1	1	1	3
Oxygen flow rate	L/min.	is in range	0.5	1	1	1	3
Nitrogen flow rate	L/min.	is in range	0	0.2	1	1	3
Power density	mW/cm^2	maximize	40	572	1	1	5

Table 6. Values provided by the program for a maximum power density

Number	Cell temperature	Hydrogen flow rate	Oxygen flow rate	Nitrogen flow rate	Power density	Desirability
1	765.3	0.98	0.98	0	580.03	1
2	786.68	1	0.82	0	565.816	0.988
3	761.05	0.93	1	0	563.791	0.985
4	765.58	1	1	0.02	561.505	0.98
5	767.74	0.87	1	0	555.82	0.97
6	782.51	1	0.74	0	553.921	0.966
7	776.1	1	0.74	0	552.077	0.963
8	787.19	1	0.7	0	545.283	0.95
9	786.37	1	0.66	0	538.609	0.937
10	779.29	1	0.5	0	507.215	0.878
11	749.86	1	1	0.2	493.251	0.852
12	755.39	1	1	0.2	492.835	0.851
13	754.06	1	1	0.18	487.534	0.841
14	734.02	0.85	1	0.2	461.558	0.792
15	723.87	0.41	1	0.2	422.936	0.72

model terms are significant. In this case A, B, and D are significant model terms. Values greater than 0.0001 indicate the model terms are not significant. The "Pred. *R* Squared" of 0.6767 is not as close to the "Adj. *R*-Squared" of 0.9921 as one might normally expect. The ANOVA results of the model is presented in tab. 7.

$$\text{Power density} = +388.9268293 - 9.9\cdot A + 40\cdot B + 28\cdot C - 14\cdot D + 91.25\cdot AB - 13.5\cdot AC - 103.25\cdot AD + 23.75\cdot BC - 148.5487805\cdot A^2 + 2.951219512\cdot B^2 + 51.95121951\cdot D^2$$

Figure 3 shows predicted power density *vs*. experimental power density from the model. It proves that the predicted data is in agreement with observed ones in the range of the operating variables.

Because of the strong effect of operating conditions at higher power density, the prediction of power density is better than that of the lower power density. The high value of adjusted $R^2 = 0.9976$ indicated that the model fits the observed data well.

The effects of cell temperatures and hydrogen flow rate on the power density are shown in fig. 4. Power density increases with increasing hydrogen flow rate. The response surface of maximum power density reaches at 750 ºC of cell temperature. After 750 ºC of the cell temperature, by increasing of cell temperatures, the power density decreases.

Table 7. The ANOVA for response surface quadratic model analysis of Design Expert 7.0

Source	Sum of squares	Df	Mean square	*F* value	p-value	Remarks
Model	3.49E+05	11	31737.57	152.47	<0.0001	significant
A	980.1	1	980.1	4.71	0.0581	
B	3200	1	3200	15.37	0.0035	
C	7840	1	7840	37.66	0.0002	
D	392	1	392	1.88	0.2032	
AB	13322.5	1	13322.5	64	<0.0001	
AC	1458	1	1458	7	0.0266	
AD	17056.9	1	17056.9	81.94	<0.0001	
BC	4512.5	1	4512.5	21.68	0.0012	
A^2	60993.46	1	60993.46	293.02	<0.0001	
B^2	24.07	1	24.07	0.12	0.7416	
D^2	7459.96	1	7459.96	35.84	0.0002	

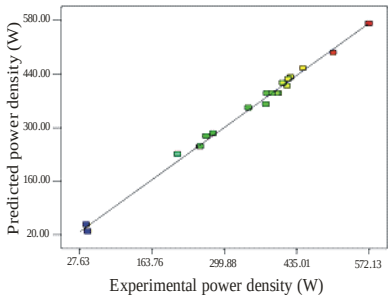

Figure 3. Plots of actual *vs.* predicted results

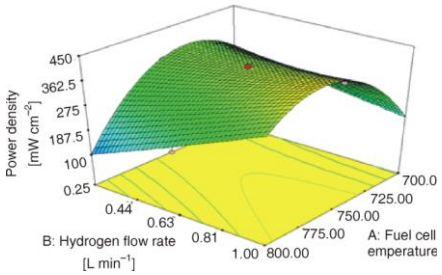

Figure 4. Power density as a function of hydrogen flow rate and cell temperature

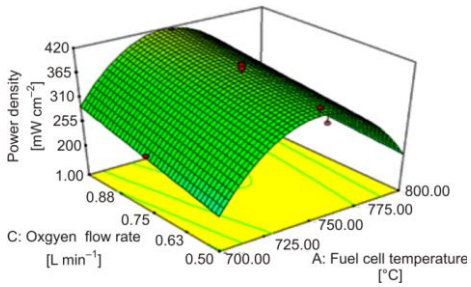

Figure 5. Power density as a function of oxygen flow rate and cell temperature

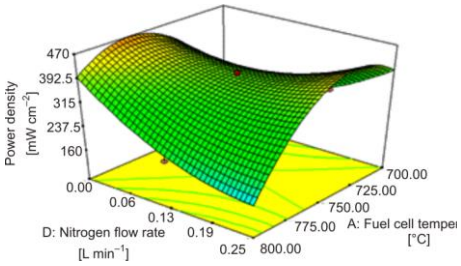

Figure 6. Power density as a function of nitrogen flow rate and cell temperature

In fig. 5, the power density is shown as a function of oxygen flow rate and cell temperature. As seen in fig. 5, increasing the oxygen flow rate does not cause a significant change in the performance of the fuel cell but reaction rate increases with increasing temperature. Additionally, the increase of temperature, hydrogen transport by increasing the anode diffusion layer contributes to performance. However, this increase is limited to the high tempera-

ture properties of the electrolyte. While the power density decreases, the response increases because of increasing of cell temperature above 750 ºC.

In fig. 6, the effect of the cell temperature and nitrogen flow rate on the power density are given. Power density is decreasing with increasing nitrogen flow rate. While the power density decreases, the response increases because of increasing of cell temperature about 720 ºC.

In fig. 7, the power density as a function of oxygen flow rate and hydrogen flow are given. While oxygen flow rate does not affect too much the performance of the cell, the increase in hydrogen flow rate is increased the power density up to a certain level. The effects of oxygen and hydrogen flow rates on the power density have been given. An increase in the cell performance is expected by increasing of the oxygen flow rate and hydrogen flow rate, but the crossover results in a decrease in the cell performance. The highest power density has been obtained at the condition of 1 L per minute hydrogen flow rate and 1 L per minute oxygen flow rate in this figure.

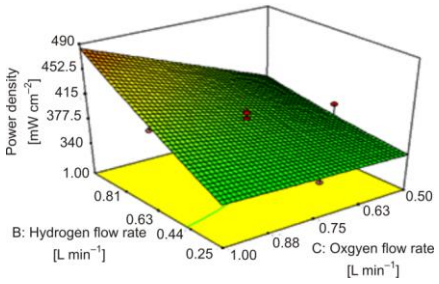

Figure 7. Power density as a function of hydrogen flow rate and oxygen flow rate

Conclusions

In this study, a 3-D electrolyte supported high temperature (700-800 ºC) planar type SOFC unit model including anode, cathode, electrolyte, fuel, air, and interconnect has been developed. The response surface method was applied to the developed model for obtaining of optimum operation conditions.

A design of experiments using Design Expert 7.0 software to find the optimum operating conditions. The main parameters (cell temperature, hydrogen flow rate, oxygen flow rate, and nitrogen flow rate) that heat management of a SOFC were investigated using RSM. This new design was used to obtain the operating conditions that originate the maximum power density.

The main conclusions are as follows.

- It was found that cell temperature and hydrogen flow rate are the basic factors affecting the power density of the SOFC.
- The power density is increased with the cell temperature in the range between 700-750 ºC but decreased between 750-800 ºC.
- Increasing the oxygen and nitrogen flow rate does not cause a significant change in the performance of the fuel cell.
- Maximum power density is observed as 573.43 mW/cm^2. This value obtained for hydrogen flow rate is 0.96 L per minute, oxygen flow rate is 0.98 L per minute, and 772.57 ºC cell temperature.

Nomenclature

c_t – total mixture molar concentration, [molm^{-3}]
D^{eff} – effective diffusivity, [m^{2}s^{-1}]
Df – degrees of freedom
e – error term
F – Faraday constant, [96500C per mol]
h – enthalpy, [kJkg^{-1}]
I – electric current, [A]
i – current density, [Acm^{-2}]
i_{ct} – charge transfer current density, [Acm^{-2}]
I – identity matrix
$\hat{i}$ – current flux vector

J – diffusion mass flux, [molm^{-2}s^{-1}]
k – conductivity, [Wm^{-1}K^{-1}]
k^{eff} – effective thermal conductivity, [Wm^{-1}K^{-1}]
M_{w} – molecular weight, [kgmol^{-1}]
n – number of moles of electrons transferred, [mol]
p – pressure, [Pa]
Q – mass source term
R_i – reaction source term, [kgm^{-3}s^{-1}]
R – electric resistance, [Ω]
S_{a} – specific surface area, [m^2]
S_{m} – source term, [kgm^{-3}s^{-1}]
S_{mass} – source term, [kgm^{-3}s^{-1}]
S_t – heat sources, [kgm^{-3}s^{-1}]
T – fluid temperature, [K]
u – velocity, [ms^{-1}]
X_{i} – main factor
x – species mass fraction
Y – response

Greek symbols

β – permeability
β_0 – constant coefficient
β_i – linear coefficients
β_{ii} – quadratic coefficients
β_{ij} – linear model coefficients
ε – porosity
ξ – shear stress tensor
η – overvoltage, [V]
κ – permeability, [m^2]
μ – dynamic viscosity, [kgm^{-1}s^{-1}]
ν – stoichiometric coefficient
ρ – density, [kgm^{-3}]
σ – electric conductivity, [1ohm^{-1}m^{-1}]
ω – weight fraction

References

[1] Kakac, S., *et al*., A Review of Numerical Modeling of Solid Oxide Fuel Cells, *International Journal for Hydrogen Energy, 32* (2007), 7, pp. 761-786
[2] Liu, Z. , *et al*., High-Performance, Ceria-Based Solid Oxide Fuel Cells Fabricated at Low Temperatures, *Journal of Power Sources, 241* (2013), Nov., pp. 454-459
[3] Wen, H., *et al*., Single Solid Oxide Fuel Cell Modeling and Optimization, *Journal of Power Sources, 196* (2011), 18, pp. 7519-7532
[4] Qua Z., *et al*., Three-Dimensional Thermo-Fluid and Electrochemical Modeling of Anode-Supported Planar Solid Oxide Fuel Cell, *Journal of Power Sources, 195* (2010), 23, pp. 7787-7795
[5] Park, J., *et al*., Computational Analysis of Operating Temperature, Hydrogen Flow Rate and Anode Thickness in Anode-Supported Flat-Tube Solid Oxide Fuel Cells, *Renewable Energy, 54* (2013), June, pp. 63-69
[6] Wen, H., *et al*., Optimization of Single SOFC Structural Design for Maximum Power, *Applied Thermal Engineering, 50* (2013), 1, pp. 12-25
[7] Wang, G., *et al*., 3-D Model of Thermo-Fluid and Electrochemical for Planar SOFC, *Journal of Power Sources, 167* (2007), 2, pp. 398-405
[8] Mauro, A., *et al*., Three-Dimensional Simulation of Heat and Mass Transport Phenomena in Planar SOFCs, *International Journal of Hydrogen Energy, 36* (2011), 16, pp. 10288-10301
[9] Costamagna, P., *et al*., Utilizatıon of Gases from Bıomass Gasification in a Reformıng Reactor Coupled to an Integrated Planar Solid Oxide Fuel Cell Simulation Analysis, *Thermal Science, 8* (2004), 2, pp. 127-142
[10] Razbani, O., *et al*., Experimental Investigation of Temperature Distribution over a Planar Solid Oxide Fuel Cell, *Applied Energy, 105* (2013), May, pp. 155-160
[11] Yan, D., *et al*., Feasibility Study of an External Manifold for Planar Intermediate-Temperature Solid Oxide Fuel Cells Stack, *International Journal of Hydrogen Energy, 38* (2013), 1, pp. 660-666
[12] Nguyen, V. N., *et al*., Long-Term Tests of a Julich Planar Short Stack with Reversible Solid Oxide Cells in Both Fuel Cell and Electrolysis Modes, *International Journal of Hydrogen Energy, 38* (2013), 11, pp. 4281-4290
[13] Jin, L., *et al*., Effect of Contact Area and that Depth between Cell Cathode and Interconnect on Stack Performance for Planar Solid Oxide Fuel Cells, *Journal of Power Sources, 240* (2013), Oct., pp. 796-805
[14] Djamel, H., *et al*., Thermal Field in SOFC Fed by Hydrogen: Inlet Gases Temperature Effect, *International Journal of Hydrogen Energy, 38* (2013), 20, pp. 8575-8583
[15] Kim, S. D., *et al*., The Effect of Gas Compositions on the Performance and Durability of Solid Oxide Electrolysis Cells, *International Journal of Hydrogen Energy, 38* (2013), 16, pp. 6569-6576
[16] Lima, H.-T., *et al*., Performance of Anode-Supported Solid Oxide Fuel Cell in Planar-Cell Channel-Type Setup, *Ceramics International, 39* (2013), Suppl. 1, pp. S659-S662

[17] Choudhuryn, A., *et al*., Application of Solid Oxide Fuel Cell Technology for Power Generation: A Review, *Renewable and Sustainable Energy Reviews, 20* (2013), Apr., pp. 430-442
[18] Secanella, M., *et al*., Computational Design and Optimization of Fuel Cells and Fuel Cell Systems: A Review, *Journal of Power Sources, 196* (2011), 8, pp. 3690-3704
[19] Ortiz-Vitoriano, N., *et al*., Optimizing Solid Oxide Fuel Cell Cathode Processing Route for Intermediate Temperature Operation, *Applied Energy, 104* (2013), Apr., pp. 984-991
[20] Bi, W., *et al*., A Key Geometric Parameter for the Flow Uniformity in Planar Solid Oxide Fuel Cell Stacks, *International Journal of Hydrogen Energy, 34* (2009), 9, pp. 3873-3884
[21] Bi, W., *et al*., Flow Uniformity Optimization for Large Size Planar Solid Oxide Fuel Cells with U-Type Parallel Channel, *Journal of Power Sources, 195* (2010), 10, pp. 3207-3214
[22] San, F. G. B., *et al*., Analysis of the Polymer Composite Bipolar Plate Properties on the Performance of PEMFC (Polymer Electrolyte Membrane Fuel Cells) by RSM (Response Surface Methodology), *Energy, 55* (2013), June, pp. 1067-1075
[23] Taymaz, I., *et al*., Application of Response Surface Methodology to Optimize and Investigate the Effects of Operating Conditions on the Performance of DMFC, *Energy, 36* (2011), 2, pp. 1155-1160
[24] ***, EG&G Technical Services Inc. Fuel Cell Handbook. USA, 2004
[25] Pasaogullari, U., Wang, C. Y., Computational Fluid Dynamics Modeling of Solid Oxide Fuel Cells, *Proceedings*, Electrochemical Society, 2003, Vol. 7, No. 8, pp. 1403-1412
[26] Wahdamea, B., *et al*., Design of Experiment Techniques for Fuel Cell Characterisation and Development, *International Journal of Hydrogen Energy, 34* (2009), 2, pp. 967-980
[27] Myers, R. H., Montgomery, D. C., Response Surface Methodology: Process and Product Optimization Using Designed Experiments, John Wiley & Sons Inc., New York, USA, 2002
[28] Bas, D., Boyaci, I. H., Modelling and Optimization I: Usability of Response Surface Methodology, *J. Food Eng., 78* (2007), 3, pp. 836-845
[29] Mišljenović, N. M., , *et al*., Optimization of the Osmotic Dehydration of Carrot Cubes in Sugar Beet Molasses, *Thermal Science, 16* (2012), 1, pp. 43-52
[30] ***, Stat-Ease, Inc. Design Expert 7 User Guide. USA; 2007
[31] Kline, S. J., McClintock, F. A., Describing Uncertainties in Single-Sample Experiments, *Mechanical Engineering, 75* (1953), 1, pp. 3-8

Paper submitted: June 17, 2013
Paper revised: February 24, 2014
Paper accepted: February 24, 2014